chemengineering

MDPI

Article

The Electrical Conductivity of a Bacterial Cellulose and Polyaniline Composite Significantly Improved by Activated Carbon: A Nano-Based Platform for Electrodes

Thanakrit Sirichaibhinyo [1], Preeyanuch Supchocksoonthorn [2], Peerasak Paoprasert [2,3] and Sarute Ummartyotin [1,3,*]

[1] Department of Materials and Textile Technology, Faculty of Science and Technology, Thammasat University, Patumtani 12120, Thailand
[2] Department of Chemistry, Faculty of Science and Technology, Thammasat University, Patumtani 12120, Thailand
[3] Center of Excellence on Petrochemical and Materials Technology, Chulalongkorn University, Bangkok 10330, Thailand
* Correspondence: sarute@tu.ac.th

Abstract: In this study, we successfully fabricated a composite sheet comprising bacterial cellulose (BC) and polyaniline (PAN), integrated with activated carbon (AC), to produce electrodes in a supercapacitor. The electrical conductivity level can be adjusted by adding AC into the composite. FTIR revealed hydrogen bonding interactions between the -OH groups of the bacterial cellulose and the -NH groups of the polyaniline. The XRD pattern showed the characteristic peak of activated carbon. The SEM showed that PAN was filled into the porous network of the bacterial cellulose. The AC was randomly distributed onto the composite's surface. The composite was thermally stable up to 200 °C. The electrical conductivity was reported to be 1.5–3.5 S/m when AC was added from 0.2 to 1 wt%. Furthermore, the specific capacitances (Cs), energy densities (Es), and power density (P) were typically reported to be 30–70 F/g, 4–11 Wh/kg, and 400–700 W/kg, respectively. Moreover, the optimization of the activated carbon ratio led to a reduction in the charge transfer resistance (R_{ct}), as demonstrated by a Nyquist plot analysis, thereby enhancing electrical conductivity. Overall, the bacterial cellulose and polyaniline composite sheet, incorporating activated carbon, exhibited excellent properties, making it a promising candidate for bioelectrode supercapacitor applications in the near future.

Keywords: nata de coco; bacterial cellulose (BC); polyaniline (PAN); activated carbon (AC); sheet composite; energy storage applications

check for updates

Citation: Sirichaibhinyo, T.; Supchocksoonthorn, P.; Paoprasert, P.; Ummartyotin, S. The Electrical Conductivity of a Bacterial Cellulose and Polyaniline Composite Significantly Improved by Activated Carbon: A Nano-Based Platform for Electrodes. *ChemEngineering* **2024**, *8*, 87. https://doi.org/10.3390/chemengineering8050087

Academic Editor: Massimiliano Lo Faro

Received: 20 June 2024
Revised: 15 August 2024
Accepted: 26 August 2024
Published: 30 August 2024

Copyright: © 2024 by the authors. Licensee MDPI, Basel, Switzerland. This article is an open access article distributed under the terms and conditions of the Creative Commons Attribution (CC BY) license (https://creativecommons.org/licenses/by/4.0/).

1. Introduction

In recent years, concerns over environmental pollutants and the shortages of natural resources have grown. Electronic materials are a major source of environmental issues [1–3], as they can turn into electronic waste after usage. From the viewpoint of sustainable development, one of the most effective strategies for dealing with this waste involves bio-based utilization. To the best of our knowledge, cellulose can be made into nano-porous networks, referred to as "nanocellulose". This novel method of cellulose production is typically related to the reverse engineering of food waste, which is referred to as bacterial cellulose extraction, or as "Acetobacter xylinum". This process offers high-purity products, excellent uniformity in size/shape, and a controllable molecular weight/repeating unit [4]. Furthermore, bacterial cellulose constitutes a nano-porous network due to its high strength and flexibility.

To meet the requirements of bacterial cellulose usage, various potential applications have been proposed, such as medical devices, chemical sensors, and flexible electrodes for electronic devices. In 2022, our research group successfully developed cellulose from

a bamboo- and polypyrrole-based composite [5]. To continue this work, we considered bacterial cellulose as a template for polyaniline formation. Then, the electrical conductivity level can be enhanced by the insertion of activated carbon. In 2024, Zheng et al. [6] developed a nanopaper supercapacitor based on cationic bacterial cellulose. They obtained a capacitance of 3988 mF/cm^2 and 97% retention after 10,000 cycles. Xie et al. [7] studied MnO_2 particles that were loaded into a bacterial cellulose network. The bacterial cellulose network exhibited a high specific surface area, and an energy density of 44.5 Wh/kg and a power density of 11,111 W/kg were obtained. Therefore, advanced methods have been used to enhance the electrical conductivity of bacterial cellulose. One way to improve the electrical conductivity of bacterial cellulose is to combine it with various conductive materials. This involves the use of conductive polymers such as polyacetylene [8], polyaniline (PAN) [9], and polythiophene [10]. The conductive polymer is integrated into a porous network throughout the bacterial cellulose, owing to the superiority of its electrical conductivity capacity. In addition to various types of conductive polymers, metal oxide particles and carbon-based materials have also generated impressive results [11–13]. They can be designed along with bacterial cellulose networks in order to form composites with the additional feature of electrical conductivity.

In this research, we presented a bacterial-cellulose-based composite sheet with added polyaniline and activated carbon. FTIR, XRD, TGA, and SEM were employed to identify the properties of the composite. After a preliminary investigation, the composite's electrical conductivity and electrochemical properties were examined. This innovative research enhanced the conductivity of the composite using polyaniline, while activated carbon was used to fill the adsorption site of the ion. The composite may be used to generate flexible and eco-friendly electrodes in the near future.

2. Experimental Sections

2.1. Materials

Bacterial cellulose was successfully extracted from a *nata de coco* product, which is locally produced in Thailand. Sodium hydroxide (NaOH) was purchased from Chem-Supply Co., Ltd. (Gillman, South Australia). The aniline monomer and ammonium persulfate (APS) were purchased from Sigma–Aldrich Co., Ltd. (Milwaukee, WI, USA). Commercial activated carbon was provided by Paoprasert's lab. It was synthesized based on the method outlined in previous studies [14]. All of the chemical reagents were of analytical grade and were used as received, without further purification.

2.2. Methods

2.2.1. Bacterial Cellulose Extraction and Purification

The *nata de coco* was washed several times with distilled water, before being blended in a blender to reduce its size. Then, the *nata de coco* was treated in a 5 wt% NaOH solution to remove impurities. The mixture was continuously stirred at 80 °C for 3 h. For the removal of the solvent, the suspension was filtered using a suction flask connected to a vacuum pump. It was subsequently rinsed with distilled water until it reached a neutral pH.

2.2.2. Fabrication of the Bacterial Cellulose (BC) and Polyaniline (PAN) Sheet with Added Activated Carbon (AC)

First, 20 mL of the bacterial cellulose suspension was poured into 50 mL of 1 M HCl solution. Then, 10 mL of the 5 mM aniline monomer was added into the mixture. It was continuously stirred at room temperature for 24 h. Then, the mixed solution was transferred into an ice-water bath, and 10 mL of 2.5 mM ammonium persulfate solution was added dropwise. Additionally, 0.2, 0.4, 0.6, 0.8, and 1 wt% of activated carbon were added to the suspension. After 6 h, the mixture was washed with distilled water several times, followed by freeze-drying for 24 h. The composites were named BC/PAN/AC-1, BC/PAN/AC-2, BC/PAN/AC-3, BC/PAN/AC-4, and BC/PAN/AC-5, obtained when

the ratios of activated carbon were 0.2, 0.4, 0.6, 0.8, and 1 wt%, respectively, as shown in Table 1.

Table 1. Compositions of the bacterial cellulose (BC) and polyaniline (PAN) sheet with added activated carbon (AC).

Sample	BC (mL)	PAN (mL)	Activated Carbon (wt%)
BC/PAN	20	10	-
BC/PAN/AC-1	20	10	0.2
BC/PAN/AC-2	20	10	0.4
BC/PAN/AC-3	20	10	0.6
BC/PAN/AC-4	20	10	0.8
BC/PAN/AC-5	20	10	1.0

2.3. Material Characterization

FTIR spectra were collected using a Nicolet iS50, Thermo Scientific, Waltham, MA, USA. It was operated using an FTIR spectrometer in the frequency range of 4000–600 cm^{-1} with 64 scans at a resolution of 4 cm^{-1}. The spectra were measured in the transmission mode.

X-ray diffraction (XRD) was carried out to study the crystalline structures of the samples. All samples were investigated using a Bruker AXS Model D8 Advance, Billerica, MA, Germany, with radiation at an angular incidence of 5–40° (2θ angle range) and a scan step of 0.02°. The operating voltage and current were 40 kV and 40 mA, respectively.

The thermal properties of the samples were measured via TGA. The TGAs of the samples were carried out in a temperature range of 30 °C to 600 °C with a heating rate of 10 °C per minute under an N_2 atmosphere.

The morphological properties of the samples were examined using field-emission scanning electron microscopy (FESEM) (JEOL JSM7800F, Japan). Prior to the investigation, the samples were sputter-coated with gold under a vacuum for 3 min to induce particle charging.

2.4. Measurement of Electrical Conductivity

For this part of the study, a four-point probe was employed. Passing a current through two outer probes and measuring the voltage through the inner probes allowed for the measurement of the substrate's resistivity. The electrical conductivity value is calculated from the four-point probe using Equation (1):

$$\sigma = \frac{1}{RsT} \quad (1)$$

where σ (Sm^{-1}) is the electrical conductivity, Rs (Ω) is the sheet resistance, and T (m) is the thickness.

2.5. Measurement of Electrochemical Performance

We used a symmetric supercapacitor in a two-electrode sandwich configuration with BC/PAN/AC sheets as the electrodes (immersed in 1 M KOH), which were separated with filtration paper. The electrochemical measurements were carried out using a two-electrode configuration in a 1 M KOH electrolyte. Platinum gauze was used as the counter electrode and a Ag/AgCl (3 M KCl) electrode acted as the reference electrode. The cyclic voltammetry (CV), the galvanostatic charge–discharge (GCD) at a current density of 0.25–2.0 A g^{-1}, and the electrochemical impedance spectroscopy (EIS) were measured using a potentiostat. CV tests were performed in a potential window between −0.2 and 0.8 V at a scan rate of 2–50 mV s^{-1}. The electrochemical impedance test was carried out at a frequency range of 0.1–10^5 Hz.

3. Results and Discussion

3.1. Development of a Bacterial Cellulose and Polyaniline Composite Sheet with Added Activated Carbon

The bacterial cellulose and polyaniline composite sheet with added activated carbon was successfully prepared. The wet composite was dried between a polytetrafluoroethylene membrane under a pressure of 58 psi, according to the standard SCAN C26:76 [15]. Then, it was freeze-dried in order to ensure the complete removal of water. All of the samples' thicknesses were estimated to be 0.05 mm.

Figure 1 illustrates the FTIR spectra of the bacterial cellulose and polyaniline composite sheet with added activated carbon. All of the characteristic peaks presented typically, with similar features. No significant peak related to activated carbon was present, due to the small amount used. However, it was noted that broad peaks were present at the wavenumbers of 3345 cm^{-1} and 2896 cm^{-1}. These peaks corresponded to OH stretching and CH stretching, respectively. The existence of an OH group was related to the hydroxyl group, suggesting that the sample could easily adhere with water molecules through H-bond linkages. On the other hand, the presence of CH stretching was due to the backbone of cellulose and polyaniline molecules [16]. Moreover, the characteristic peaks at the wavenumbers of 1056 cm^{-1} and 1029 cm^{-1} were present due to N-H stretching. They correspond to an amine group. Furthermore, the presence of a wave number at 1156 cm^{-1} indicates hydrogen bonding between bacterial cellulose and aniline. These peaks signify the formation of polyaniline. These results demonstrate the successful incorporation of polyaniline into the cellulose matrices.

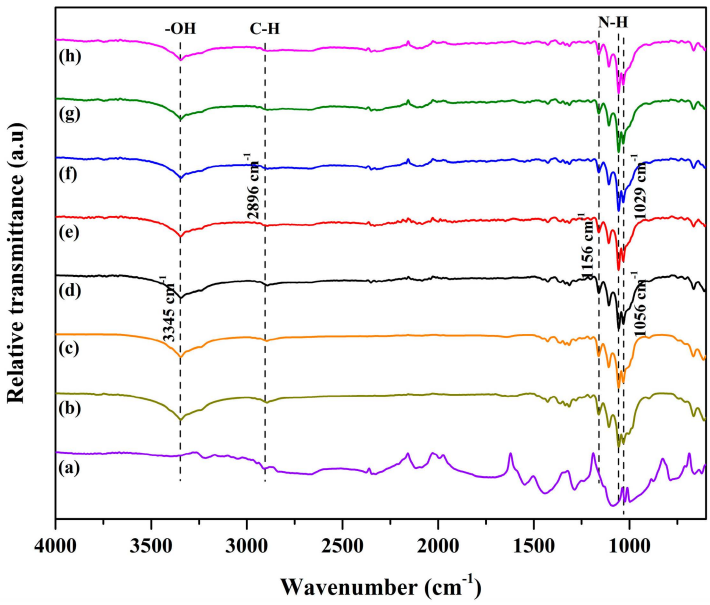


Figure 1. The FTIR spectra of (a) polyaniline, (b) bacterial cellulose, (c) the bacterial cellulose and polyaniline composite sheet, and (d–h) the composite sheet with the addition of activated carbon at 0.2, 0.4, 0.6, 0.8, and 1.0 wt%.

X-ray diffraction was employed to evaluate the crystallinity of the composite sheet. Figure 2 shows the XRD pattern of the bacterial cellulose and polyaniline composite sheet with added activated carbon. It was observed that, in the case of the pristine bacterial cellulose and polyaniline sheet, only two diffraction angles were observed at 2θ angles of 14.8 and 22.5. These angles typically refer to diffraction of 110 and 020, respectively. They belong to cellulose I. This corresponds to JCPDS No. 50-2241. However, when the activated carbon was integrated into the composite sheet, the intensity of the sheet was reduced. This was probably because the crystallinity of the activated carbon was slightly high. The intensity of the peak at the diffraction angle of 26.5° was evident. This finding

corresponded with JCPDS No. 41-1487. This peak corresponds to a diffraction plane of 002 [17]. This angle overlapped with the cellulose I angle, suggesting that the intensity would increase proportionally with the amount of activated carbon added. Additionally, the diffraction plane of 110 decreased upon the addition of activated carbon, indicating its incorporation into the structure and the obscuring of the cellulose band.

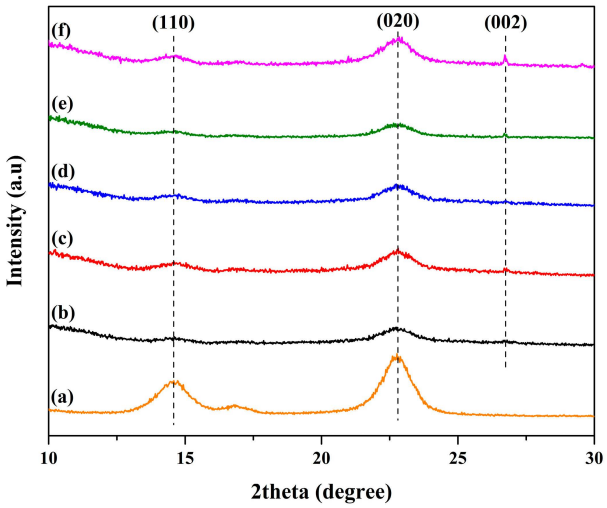


Figure 2. The XRD patterns of (a) the bacterial cellulose and polyaniline composite sheet with the addition of activated carbon and (b–f) 0.2, 0.4, 0.6, 0.8, and 1.0 wt%.

In order to ensure the thermal stability of the composite sheet, thermogravimetric analysis (TGA) was employed. Figure 3 shows the thermal decomposition behavior of the composite sheet with the addition of activated carbon. It was observed that, based on the applied temperature, the characteristic curve of thermal decomposition can be divided into three distinct regions. From an ambient temperature to 250 °C, no weight loss was observed. This confirms that the composite was thermally stable up to 250 °C. When the temperature was increased to 250–400 °C, a broad region of weight loss was observed. This temperature region was related to the pyrolysis process. The sample was changed into volatile gasses such as CO_2 and NO_x. The change in weight loss depended on the activated carbon. The activated carbon influenced the material's improved thermal resistance. After that, when the temperature region was increased upwards of 400 °C, weight loss was more or less constant. The rest comprised char/residual material.

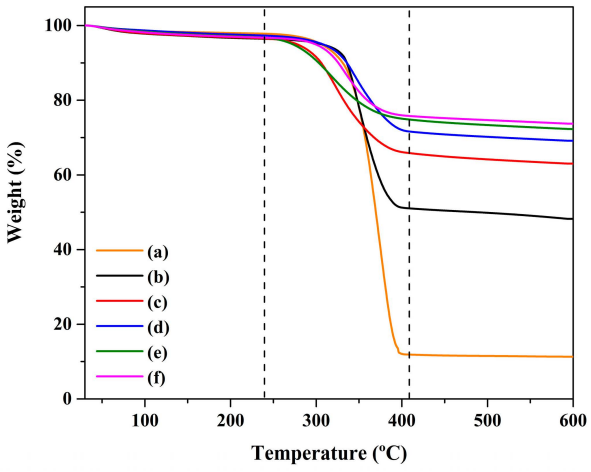


Figure 3. The thermal decomposition behavior of (a) the bacterial cellulose and polyaniline composite sheet with added activated carbon and (b–f) 0.2, 0.4, 0.6, 0.8, and 1.0 wt%.

To examine the morphology of the composite, FESEM analyses were performed, as depicted in Figure 4. The morphology of BC presented as a nano-porous network of cellulose. Conversely, the BC/PAN sheet exhibited slightly more tightly packed fibers, which can potentially be attributed to the interaction between BC and PAN. Furthermore, the BC/PAN/AC composite sheet exhibited activated carbon particles inserted into the porous network of BC. With the addition of activated carbon, these particles migrated into the inner network of BC/PAN and adhered to the surfaces of the BC/PAN sheets. This finding is in agreement with the XRD results. The intensity of the BC composite sheet was relatively low.

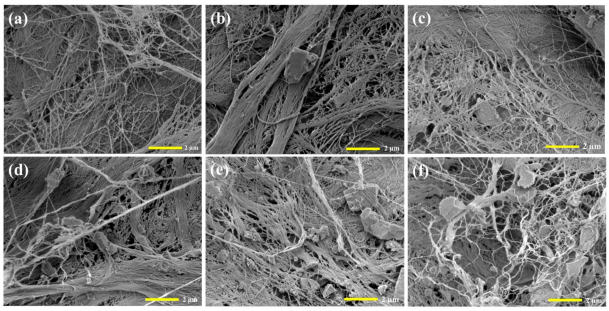


Figure 4. FE-SEM images of (**a**) the BC/PAN sheet and (**b**–**f**) the 0.2, 0.4, 0.6, 0.8, and 1.0 wt% BC/PAN/AC sheet composites.

Figure 5 shows the nitrogen adsorption–desorption isotherms and the pore-size distribution. The BET surface area (S_{BET}) and the pore volume of the composite increased proportionally with the ratio of activated carbon. The incorporation of activated carbon enhanced the sheet's porosity. Pore diameters of 1.5 nm indicated the presence of a microporous structure. Notably, BC/PAN/AC-5 exhibited the highest S_{BET} (740.05 m^2g^{-1}), with a pore diameter of approximately 1.4584 nm. Moreover, the N_2 adsorption–desorption behavior of the BC/PAN/AC composite sheet exhibited type I isotherms, suggesting Langmuir (monolayer) adsorption characteristics [18].

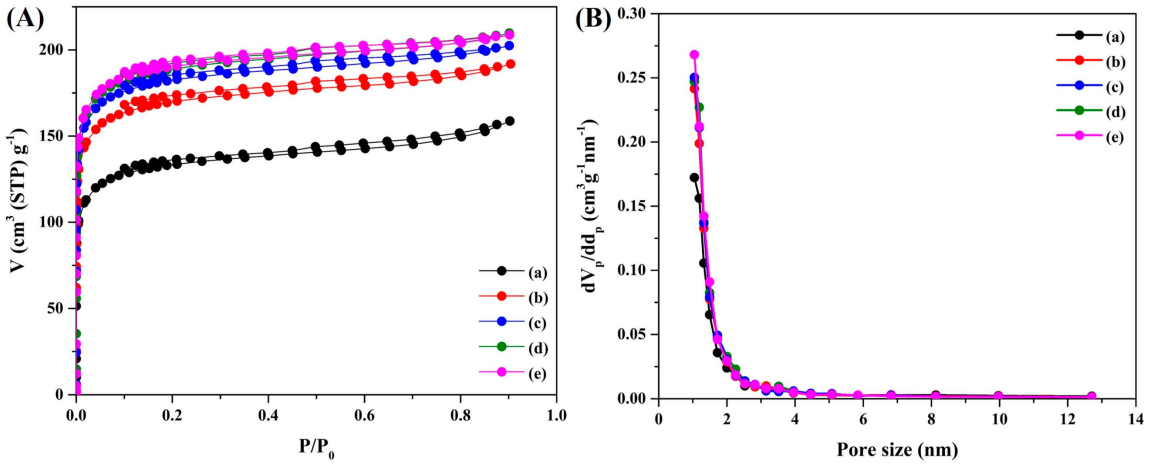


Figure 5. (**A**) The nitrogen adsorption–desorption isotherms and (**B**) the pore-size distribution of the BC/PAN/AC composite sheet. (a) the BC/PAN sheet and (b–e) the 0.2, 0.4, 0.6, 0.8, and 1.0 wt% BC/PAN/AC composite sheets.

3.2. Evaluation of Electrical and Electrochemical Properties

To design the electrode, the electrical conductivity was first determined using the four-point probe technique, as depicted in Figure 6. An investigation of the bacterial cellulose was carried out, and high resistivity was observed. Furthermore, in the case of

the composite sheet, a significant increase in electrical conductivity was observed with respect to the amount of activated carbon used. The introduction of activated carbon further enhanced the electrical conductivity, establishing the BC/PAN sheet with activated carbon as an excellent candidate for an electrode.

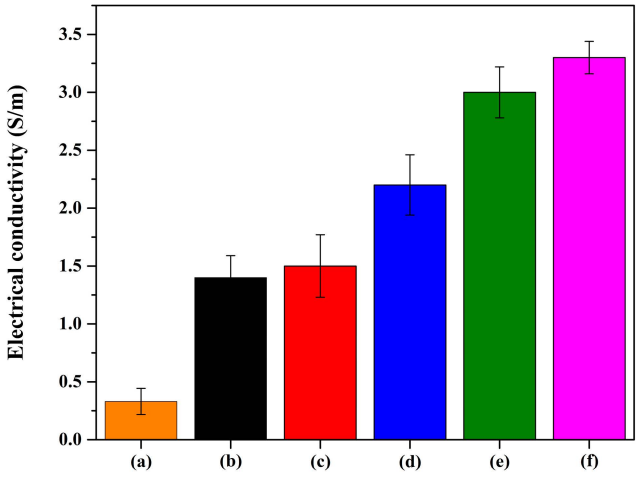


Figure 6. The electrical conductivity of the BC/PAN sheet and BC/PAN with different ratios of activated carbon. (a) The BC/PAN sheet and (b–f) the 0.2, 0.4, 0.6, 0.8, and 1.0 wt% BC/PAN/AC composite sheets.

Table 2 presents the conductivity levels of our composite in comparison to those reported in the literature. Specifically, the conductivity of our composite, consisting of bacterial cellulose/polyaniline with 1 wt% activated carbon, was recorded at 0.0325 S/m. This value aligns closely with findings from previous studies. The versatility of the conductivity level means that the composite can be further developed for potential applications, such as flexible electrodes for biosensors and supercapacitors.

Table 2. A comparison of the conductivity level of the bacteria cellulose/polyaniline/activated carbon composite and the previously reported conductive cellulose composites.

Materials	Conductivity Level (S/cm)	Application	References
Bacteria cellulose/polyaniline/titanium dioxide	0.037	Bioanode in microbial fuel cell	[19]
Cellulose/graphene/polyaniline	1.66	Supercapacitors	[20]
Cellulose/reduced graphene oxide/polyaniline	3.1	Biosensors, supercapacitors	[21]
Polyaniline composites with lotus-leaf-derived carbon	3.57×10^{-3}	Supercapacitor	[22]
MXene (Ti_3C_2Tx)/cellulose nanofiber/polyaniline	N/A	Supercapacitor	[23]
Carbon fiber/graphene/bacterial cellulose/polyaniline	N/A	Supercapacitor	[24]
BC/PAN/AC sheet composites	0.0325	Supercapacitors	Our work

The electrochemical performance of the composite was evaluated using a two-electrode system in a 1 M KOH solution. Figure 7A–BF depicts the CV curves of the composite across varying scan rates ranging from 5 to 100 mVs^{-1}. The rectangular form of the CV curves remained consistent across different scan rates, suggesting the presence of electric double-layer capacitive characteristics. It is evident that increasing scan rates result in a positive shift in the oxidation peaks and a negative shift in the reduction peaks, which are attributed to heightened internal resistance. Additionally, the current intensity increases as the scan rate increases. The specific capacitance (Cs, F g^{-1}) value is calculated from the CV values using Equation (2):

$$Cs = \frac{\int IVdV}{2\ \mu m \Delta V} \quad (2)$$

where $\int$ IVdV is an integral area of a CV plot (a graph between current (A) and potential (V)), μ is the scan rate (V s^{-1}), m is the mass of active materials on the working electrode (g), and ΔV is the potential window (V). The energy density (E, Wh kg^{-1}) and power density (P, W kg^{-1}) of the supercapacitor can be calculated using Equations (3) and (4), respectively:

$$E = \frac{1000}{3600 \times 2} Cs(\Delta V)^2; \quad (3)$$

$$P = \frac{E}{\Delta t}(3600) \quad (4)$$

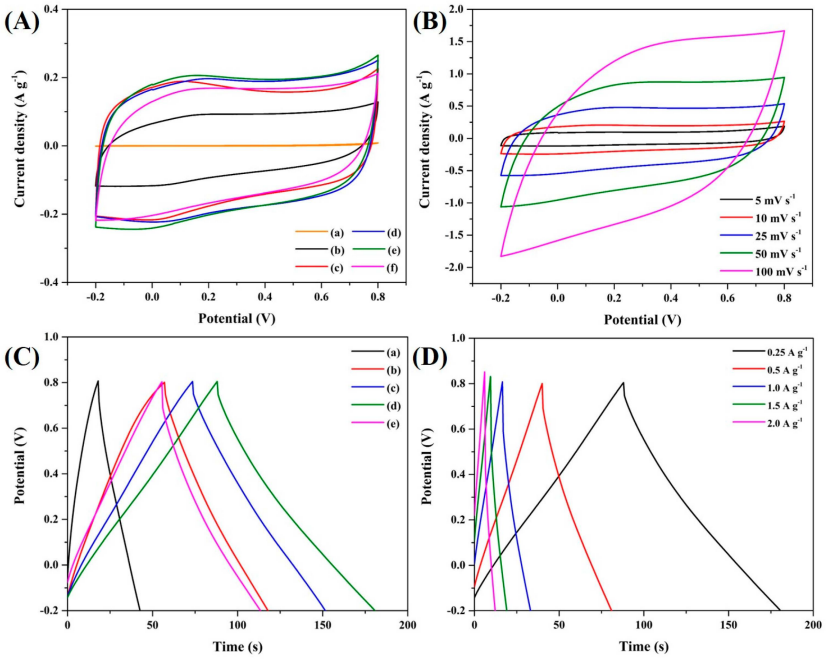


Figure 7. The CV curves of (**A**) a BC/PAN/AC sheet composite at a scan rate of 10 mVs^{-1}, (**B**) BC/AC−4 at different scan rates, (**C**) the galvanostatic charge–discharge curves of the BC/PAN/AC sheet composite at 0.25 A g^{-1}, and (**D**) BC/AC−4 at different current densities.

An analysis of the graph reveals that the graph area increases proportionally with the amount of added activated carbon. However, the excessive augmentation of activated carbon content may lead to an overabundance being incorporated into the structure, as indicated by the SEM analysis. Consequently, it is evident that, in BC/PAN/AC-5, the Cs value is lower than that of BC/PAN/AC-4. The CV curves of BC-AC/4 (0.8 wt% activated carbon) suggest superior ion conductivity in the added-carbon material compared to the one without activated carbon. It exhibited the highest Cs of 73.051 F g^{-1} and an E of 10.21 Wh kg^{-1} (Table 3). The enhanced performance of the BC-AC/4 electrodes was probably due to the existence of activated carbon inside of the bacterial cellulose. The charge–discharge profiles of the BC/PAN/AC electrodes at the current density of 0.25 A g^{-1} are depicted in Figure 7C; they have a symmetric, triangular shape, indicating their exceptional reversible characteristics during the charge–discharge process and exhibiting electric double-layer capacitor (EDLC) behaviors due to the activated carbon [25]. Lower current densities were associated with prolonged charge–discharge durations, suggesting an increase in Cs as the current density decreases. As the current density increases, as shown in Figure 7D, the duration of the charge–discharge process for each electrode diminishes; this is primarily due to the inadequate utilization of the active components within the short time span. With limited time available, ions fail to penetrate deeper into the electrodes, leading to restricted electrochemical reactions occurring predominantly at the surfaces. The charge–discharge curves of the BC/PAN/AC−4 electrodes at current densities of

0.25 A g^{-1} exhibit the longest discharge time, leading them to have the highest specific capacitance compared to other electrodes. This indicates their enhanced electrochemical reversibility. Moreover, the discharge curves of BC/PAN/AC−4 indicate the lowest voltage drop (referred to as the IR drop), due to the internal resistance of the electrodes.

Table 3. The specific capacitances (Cs), energy densities (Es), and power density (P) of BC/PAN with different ratios of activated carbon.

Condition	Cs (F g^{-1}) at 10 mV s^{-1}	E (Wh kg^{-1})	P (W kg^{-1})
BC/PAN/AC-1	33.174	4.61	677.01
BC/PAN/AC-2	60.443	8.39	499.53
BC/PAN/AC-3	70.091	9.73	449.29
BC/PAN/AC-4	73.051	10.21	397.30
BC/PAN/AC-5	63.283	8.79	550.29

To determine the electrochemical characteristics of the aforementioned electrodes, an electrochemical impedance spectroscopy (EIS) analysis was conducted within the frequency range of 0.1 to 10^5 Hz. Figure 8a shows the Nyquist plots of the composite. These plots exhibit a semicircle in the high-frequency region (where the semicircle's diameter signifies the charge transfer resistance, R_{ct}); the point where the Nyquist curve intersects with the Z' axis reveals the electrolyte resistance (Rs), and a linear segment in the low-frequency region indicates the capacitive behavior. Notably, the BC/PAN/AC−4 electrode exhibited a semicircle within the high-frequency range and a straight sloping line within the low-frequency region. Additionally, the diameter of the semicircle indicated a low charge transfer resistance (R_{ct}) of 2.504 Ω, which played a crucial role in achieving a relatively high specific power density. Meanwhile, the BC/PAN/AC−1 electrode showed the semicircle with the largest diameter, indicating a charge transfer resistance (R_{ct}) of 9.846 Ω that related to specific capacitance. These results indicate that the BC/PAN/AC−4 electrode exhibited the most elevated interface conductivity levels between the electrolyte and the electrode/current collector, along with reduced internal resistance within the supercapacitor setup [26].

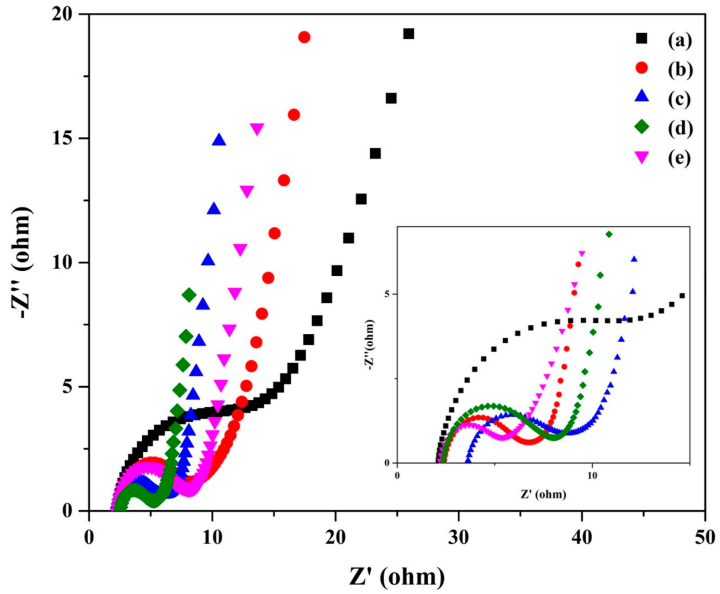


Figure 8. The Nyquist plots of the BC/PAN/AC sheet composite in 1 M KOH electrolyte. (a) the BC/PAN sheet and (b–f) the 0.2, 0.4, 0.6, 0.8, and 1.0 wt% BC/PAN/AC sheet composites.

Table 4 presents the specific capacitance levels of our composite compared to examples in the literature. Specifically, our composite exhibited a specific capacitance of 73.051 F/g. This result is similar to results reported in other studies.

Table 4. A comparison of the specific capacitance level of the bacteria cellulose/polyaniline/activated carbon composite and of previously reported cellulose composites.

Materials	Specific Capacitance (F g^{-1})	Current Density (A g^{-1})	References
Graphene oxide/bacterial cellulose film	65.9	0.4	[27]
Co_3O_4 nanoparticles incorporated into a cellulose nanofiber	80	1.0	[28]
TEMPO-oxidized nanocellulose-stabilized carbon nanotubes	65	0.4	[29]
Ni_3S_2/carbon nanofibers derived from bacterial cellulose	56.6	1.0	[30]
NH_4CoPO_4/bacterial cellulose composite	43.3	0.25	[31]
BC/PAN/AC sheet composites	73.051	0.25	This work

4. Conclusions

We successfully fabricated a composite sheet comprising bacterial cellulose (BC) and polyaniline (PAN), integrated with activated carbon (AC). PAN was used to fill a porous network of bacterial cellulose, generating a significantly high conductivity level. AC was inserted into the composite to enhance the specific surface area for the adsorption site of the ion. The activated carbon was randomly distributed into the porous network of the bacterial cellulose and polyaniline composite. It presented as an island particle located in between the bacterial cellulose networks. The FTIR spectra and XRD pattern confirmed that the composite typically presented similar structural properties to pristine bacterial cellulose. The composite was thermally stable up to 250 °C. The specific surface area and pore diameter were estimated to be 740 m^2/g and 1.5 nm, respectively. The electrical conductivity was reported to be 1.5–3.5 S/m when AC was inserted from 0.2 to 1 wt%. The specific capacitance (Cs), energy density (E), and power density (P) were typically reported to be 30–70 F/g, 4–11 Wh/kg, and 400–700 W/kg, respectively. It is evident that, with the addition of AC, the composite exhibited excellent electrochemical properties. We therefore conclude that the composite sheet comprising bacterial cellulose (BC) and polyaniline (PAN), integrated with activated carbon (AC), is suitable to be used in flexible electrodes in the near future.

Author Contributions: T.S.: validation, writing—original draft, methodology. P.S.: methodology. P.P.: writing—review and editing. S.U.: conceptualization, writing—review and editing, supervision, resources. All authors have read and agreed to the published version of the manuscript.

Funding: Thailand Science Research and Innovation Fundamental Fund Fiscal year 2024, Thammasat University.

Data Availability Statement: Data supporting the study are available from the authors upon reasonable request.

Acknowledgments: This work was supported by the Thailand Science Research and Innovation Fundamental Fund, Fiscal year 2024, Thammasat University. The authors would like to acknowledge the support provided by Thammasat University Research Unit in Textile and Polymer Chemistry. Finally, S.U. would like to acknowledge the support of the Hub of Talent: Sustainable Materials for Circular Economy, National Research Council of Thailand (NRCT).

Conflicts of Interest: The authors declare that they have no known competing financial interests or personal relationships that could have appeared to influence the work reported in this article.

References

1. Dai, S.; Zhang, W.; Xia, T.; Hu, H.; Zhang, Z.; Li, X. Insight into faradaic mechanism of NiCo-CHH microspheres in high-performance Ni-Cu batteries. *Scr. Mater.* **2022**, *215*, 114691. [CrossRef]
2. Zhang, K.; Wang, H.; Du, X.; Dai, S.; Wang, Y.; Xu, T.; Liu, M.; Cheng, S. Reaction Mechanism and Structural Evolution of Tunnel-Structured KCu7S4 Nanowires in Li+/Na+-Ion Batteries. *Adv. Funct. Mater.* **2024**, *34*, 2407105. [CrossRef]

3. Qu, J.; Bai, Y.; Li, X.; Song, K.; Zhang, S.; Wang, X.; Wang, X.; Dai, S. Rational design of NiSe2@rGO nanocomposites for advanced hybrid supercapacitors. *J. Mater. Res. Technol.* **2021**, *15*, 6155–6161. [CrossRef]
4. Chantereau, G.; Sharma, M.; Abednejad, A.; Vilela, C.; Costa, E.M.; Veiga, M.; Antunes, F.; Pintado, M.M.; Sèbe, G.; Coma, V.; et al. Bacterial nanocellulose membranes loaded with vitamin B-based ionic liquids for dermal care applications. *J. Mol. Liquids* **2020**, *302*, 112547. [CrossRef]
5. Khamwongsa, P.; Wongjom, P.; Cheng, H.; Lin, C.C.; Ummartyotin, S. Significant enhancement of electrical conductivity of conductive cellulose derived from bamboo and polypyrrole. *Compos. Part C Open Access* **2022**, *9*, 100314. [CrossRef]
6. Zheng, W.; Fan, L.; Zhou, J.; Meng, Z.; Ye, D.; Xu, J. Flexible, ultrathin and integrated nanopaper supercapacitor based on cationic bacterial cellulose. *Int. J. Biol. Macromol.* **2024**, *256*, 128497. [CrossRef]
7. Xie, X.; Zhang, J.; Du, X.; Kimura, H.; Ni, C.; Hou, C.; Zhang, Y.; Sun, X.; Yang, X.; Du, W. Morphology evolution of bacterial cellulose carbon and loaded with MnO_2 microspheres for high performance supercapacitors. *J. Alloys Compd.* **2024**, *994*, 174713. [CrossRef]
8. Shen, Y.-H.; Yadav, R.; Wong, A.J.; Balzer, A.H.; Epps, T.H.; Sumerlin, B.S.; Veige, A.S. Fibril size control, tensile strength, and electrical properties of cyclic polyacetylene. *React. Funct. Polym.* **2024**, *195*, 105810. [CrossRef]
9. Sun, P.; Shen, X.; Xu, P.; Huang, W.; Xu, Q. Conductive polyaniline film synthesized through in-situ polymerization as a conductive seed layer for hole metallization of printed circuit boards. *Appl. Surf. Sci.* **2024**, *655*, 159649. [CrossRef]
10. Shindalkar, S.S.; Reddy, M.; Singh, R.; Nainar, M.A.M.; Kandasubramanian, B. Polythiophene blends and composites as potential energy storage materials. *Synth. Met.* **2023**, *299*, 117467. [CrossRef]
11. Li, E.; Liu, R.; Huang, S.; Mei, J.; Xu, J.; Yuan, G. Flexible N-doped active carbon/bacterial cellulose paper for supercapacitor electrode with high areal performance. *Synth. Met.* **2017**, *226*, 104–112. [CrossRef]
12. Hunge, Y.M.; Yadav, A.A.; Kang, S.-W.; Kim, H.; Fujishima, A.; Terashima, C. Nanoflakes-like nickel cobaltite as active electrode material for 4-nitrophenol reduction and supercapacitor applications. *J. Hazard. Mater.* **2021**, *419*, 126453. [CrossRef] [PubMed]
13. Yadav, A.A.; Hunge, Y.M.; Ko, S.; Kang, S.-W. Chemically Synthesized Iron-Oxide-Based Pure Negative Electrode for Solid-State Asymmetric Supercapacitor Devices. *Materials* **2022**, *15*, 6133. [CrossRef] [PubMed]
14. Jorn-am, T.; Pholauyphon, W.; Supchocksoonthorn, P.; Sirisit, N.; Chanthad, C.; Manyam, J.; Liang, X.; Song, S.; Paoprasert, P. High-performance supercapacitors using synergistic hierarchical Ni-doped copper compounds/activated carbon composites with MXenes and carbon dots as simultaneous performance enhancers. *Electrochim. Acta* **2023**, *447*, 142147. [CrossRef]
15. Piili, H. A study on usage of on-site multi-monitoring system in laser processing of paper materials. *Physics Procedia* **2015**, *78*, 147–156. [CrossRef]
16. Liu, R.; Ma, L.; Huang, S.; Mei, J.; Xu, J.; Yuan, G. Large areal mass, flexible and freestanding polyaniline/bacterial cellulose/graphene film for high-performance supercapacitors. *RSC Adv.* **2016**, *6*, 107426–107432. [CrossRef]
17. Kalagatur, N.K.; Karthick, K.; Allen, J.A.; Nirmal Ghosh, O.S.; Chandranayaka, S.; Gupta, V.K.; Krishna, K.; Mudili, V. Application of activated carbon derived from seed shells of Jatropha curcas for decontamination of zearalenone mycotoxin. *Front. Pharmacol.* **2017**, *8*, 308339. [CrossRef]
18. Thongsai, N.; Hrimchum, K.; Aussawasathien, D. Carbon fiber mat from palm-kernel-shell lignin/polyacrylonitrile as intrinsic-doping electrode in supercapacitor. *Sustain. Mater. Technol.* **2021**, *30*, e00341. [CrossRef]
19. Truong, D.H.; Dam, M.S.; Bujna, E.; Rezessy-Szabo, J.; Farkas, C.; Vi, V.N.H.; Csernus, O.; Nguyen, V.D.; Gathergood, N.; Friedrich, L. In situ fabrication of electrically conducting bacterial cellulose-polyaniline-titanium-dioxide composites with the immobilization of Shewanella xiamenensis and its application as bioanode in microbial fuel cell. *Fuel* **2021**, *285*, 119259. [CrossRef]
20. Luo, H.; Dong, J.; Zhang, Y.; Li, G.; Guo, R.; Zuo, G.; Ye, M.; Wang, Z.; Yang, Z.; Wan, Y. Constructing 3D bacterial cellulose/graphene/polyaniline nanocomposites by novel layer-by-layer in situ culture toward mechanically robust and highly flexible freestanding electrodes for supercapacitors. *Chem. Eng. J.* **2018**, *334*, 1148–1158. [CrossRef]
21. Kabiri, R.; Namazi, H. Synthesis of cellulose/reduced graphene oxide/polyaniline nanocomposite and its properties. *Int. J. Polym. Mater. Polym. Biomater.* **2016**, *65*, 675–682. [CrossRef]
22. Gao, P.; Yuan, P.; Wang, S.; Shi, Q.; Zhang, C.; Shi, G.; Xing, Y.; Shen, B. Preparation and comparison of polyaniline composites with lotus leaf-derived carbon and lotus petiole-derived carbon for supercapacitor applications. *Electrochim. Acta* **2024**, *486*, 144112. [CrossRef]
23. Yuan, T.; Zhang, Z.; Liu, Q.; Liu, X.-T.; Miao, Y.-N.; Yao, C.-L. MXene (Ti_3C_2Tx)/cellulose nanofiber/polyaniline film as a highly conductive and flexible electrode material for supercapacitors. *Carbohydr. Polym.* **2023**, *304*, 120519. [CrossRef] [PubMed]
24. Tan, H.; Navik, R.; Liu, Z.; Xiang, Q.; Zhao, Y. Preparation of high load carbon fiber/graphene/bacterial cellulose/polyaniline electrodes facilitated by plasma towards high capacitive supercapacitors. *Chem. Phys. Lett.* **2022**, *802*, 139741. [CrossRef]
25. Lei, C.; Amini, N.; Markoulidis, F.; Wilson, P.; Tennison, S.; Lekakou, C. Activated carbon from phenolic resin with controlled mesoporosity for an electric double-layer capacitor (EDLC). *J. Mater. Chem. A* **2013**, *1*, 6037–6042. [CrossRef]
26. Chaisit, S.; Chanlek, N.; Khajonrit, J.; Sichumsaeng, T.; Maensiri, S. Preparation, characterization, and electrochemical properties of KOH-activated carbon from cassava root. *Mater. Res. Express* **2020**, *7*, 105605. [CrossRef]
27. Guan, F.; Chen, S.; Sheng, N.; Chen, Y.; Yao, J.; Pei, Q.; Wang, H. Mechanically robust reduced graphene oxide/bacterial cellulose film obtained via biosynthesis for flexible supercapacitor. *Chem. Eng. J.* **2019**, *360*, 829–837. [CrossRef]
28. Rabani, I.; Yoo, J.; Kim, H.-S.; Hussain, S.; Karuppasamy, K.; Seo, Y.-S. Highly dispersive Co_3O_4 nanoparticles incorporated into a cellulose nanofiber for a high-performance flexible supercapacitor. *Nanoscale* **2021**, *13*, 355–370. [CrossRef]

29. Wu, Y.; Sun, S.; Geng, A.; Wang, L.; Song, C.; Xu, L.; Jia, C.; Shi, J.; Gan, L. Using TEMPO-oxidized-nanocellulose stabilized carbon nanotubes to make pigskin hydrogel conductive as flexible sensor and supercapacitor electrode: Inspired from a Chinese cuisine. *Compos. Sci. Technol.* **2020**, *196*, 108226. [CrossRef]
30. Yu, W.; Lin, W.; Shao, X.; Hu, Z.; Li, R.; Yuan, D. High performance supercapacitor based on Ni_3S_2/carbon nanofibers and carbon nanofibers electrodes derived from bacterial cellulose. *J. Power Sources* **2014**, *272*, 137–143. [CrossRef]
31. Wannasen, L.; Swatsitang, E.; Pinitsoontorn, S. Flexible supercapacitors based on mesoporous nanocrystalline cobalt ammonium phosphates and bacterial cellulose composite electrode. *Int. J. Energy Res.* **2021**, *45*, 3075–3088. [CrossRef]

Disclaimer/Publisher's Note: The statements, opinions and data contained in all publications are solely those of the individual author(s) and contributor(s) and not of MDPI and/or the editor(s). MDPI and/or the editor(s) disclaim responsibility for any injury to people or property resulting from any ideas, methods, instructions or products referred to in the content.